The $z \sim 1.2$ Galaxy Luminosity Function from The LCIR Survey

H.-W. Chen[1], P. J. McCarthy[1], R. O. Marzke[2], R. G. Carlberg[3], A. E. Firth[4], S. E. Persson[1], R. G. McMahon[4], O. Lahav[4], P. Martini[1], R. S. Ellis[5], R. G. Abraham[3], A. Oemler[1], R. S. Somerville[4]

[1]*Carnegie Observatories, 813 Santa Barbara St, Pasadena, CA 91101, U.S.A.*

[2]*Department of Astronomy and Physics, San Francisco State University, San Francisco, CA 94132-4163, U.S.A.*

[3]*Department of Astronomy, University of Toronto, Toronto ON, M5S 3H8 Canada*

[4]*Institute of Astronomy, Cambridge CB3 OHA, England, UK*

[5]*Department of Astronomy, Caltech 105-24, Pasadena, CA 91125, U.S.A.*

Abstract.

We present results from the Las Campanas Infrared Survey, designed to identify a statistically significant sample of $z \gtrsim 1$ galaxies using photometric redshift techniques. Here we summarize the design and strategies of the survey and present the first estimate of the galaxy luminosity function at $z \gtrsim 1$ based on H-band selected galaxies identified in our survey. Results of number count studies and luminosity function measurements indicate that most early-type galaxies were already in place by $z \sim 1.2$ with a modest space density evolution and a mild luminosity evolution over that expected from passive evolution.

1 Introduction

Evolved high-redshift galaxies hold the key to addressing two fundamental issues in observational cosmology: First, when did the bulk of star formation and mass assembly occur? Second, how does the space density of galaxies evolve with time? Because different galaxy formation scenarios have distinct predictions for the space densities and masses of galaxies at redshifts beyond one, comparisons of statistical properties of evolved high-redshift galaxies and local ellipticals may provide a direct means of discriminating between competing galaxy formation scenarios ([8]). Previous studies of evolved galaxies have yielded inconsistent measurements of their space density (see [2] for a list of references) due to a strong field-to-field variation in the surface density ([4, 13, 14, 6]) and various selection biases ([17]). Evolved galaxies may be characterized by their intrinsically red colors due to the lack of ongoing star formation that provides most of the UV light in typical galaxy spectral energy distributions, but confusions may arise because of the presence of dusty star-forming galaxies that exhibit similar colors.

We have been conducting the Las Campanas Infrared (LCIR) Survey in the past two years. It is a deep near-infrared and optical imaging survey of distant galaxies over one square degree of sky at high galactic latitudes ([12, 13, 14, 2]). This program utilizes one of the largest near-infrared cameras available (CIRSI;[1]) that produces an image of $13' \times 13'$ contiguous field of view in a sequence of four pointings. The survey is designed to identify a large number of red galaxies at $z > 1$ using photometric redshift techniques. The primary objectives of the program are (1) to examine the nature of the red galaxy population and identify evolved galaxies at $z > 1$, (2) to study the space density and luminosity evolution of evolved galaxies at $z \lesssim 2$, and (3) to measure the spatial clustering of evolved high-redshift galaxies ([13, 14, 6]), thereby inferring merging rates of these galaxies for constraining theoretical models. Here we summarize the survey design and present initial results from comparing optical and near-infrared colors, number density and luminosity evolution between galaxies at different redshifts.

2 Current Status of the Survey

We have completed an H-band imaging survey in six distinct high galactic latitude fields, covering 1.1 square degrees of sky, to a mean $5\,\sigma$ detection limit in a four arcsecond diameter aperture of $H \sim 20.8$.

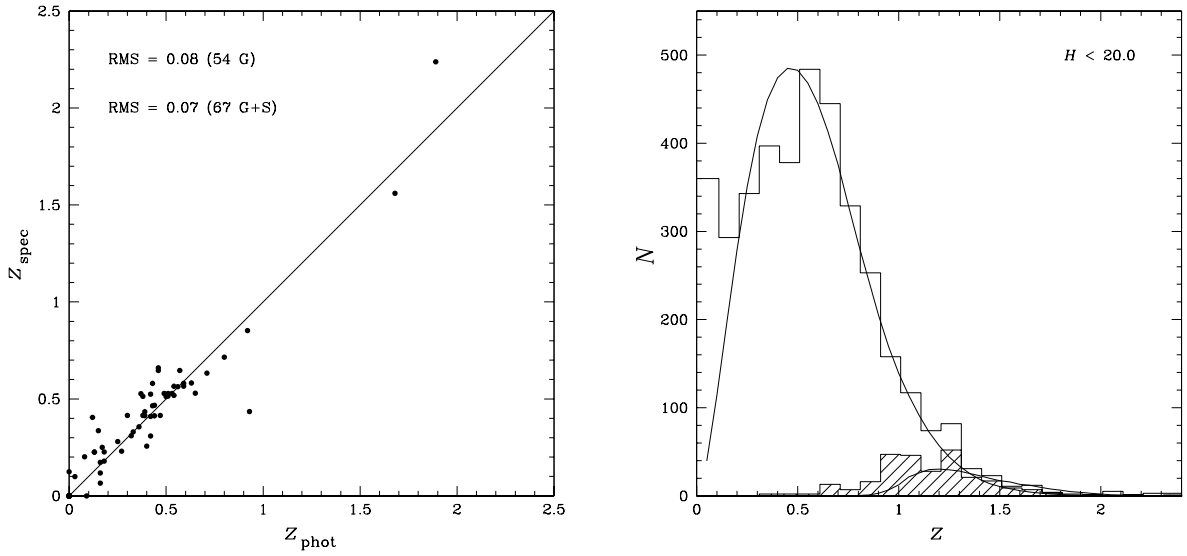

Figure 1: (a) Comparison of photometric redshifts $z_{\rm phot}$ and spectroscopic redshifts $z_{\rm spec}$ for 13 stars and 54 galaxies observed spectroscopically in the HDFS. (b) Redshift histogram of the H-band detected galaxies in the HDFS region. The shaded part indicates the redshift distribution of the $I-H \gtrsim 3$ galaxies. Solid curves indicate the predicted redshift distribution based on the model that best fits the differential surface density measurements.

We have also obtained complementary optical images of these fields to consistent depths required to identify red galaxies with $R-K_s \gtrsim 5$ or $I-H \gtrsim 3$ ([12, 2]). Details of the H-band survey status and sample photometric catalogs are presented in [2]. The current survey depths allow us to identify evolved galaxies that are more than one magnitude fainter than an $L*$ elliptical galaxy at $z \sim 1$.

We have initiated a K_s-band imaging survey of the six fields using a re-imaging camera developed by Persson et al. ([15]) that provides an effective cold stop, extending the operational range of CIRSI to the K_s band. The primary goal of the K_s-band survey is to extend the redshift range probed by the H-band survey, in order for us to identify sub-L_* galaxies at $z \gtrsim 1.5$. We have observed ≈ 320 square arcminutes of sky to a mean $5\,\sigma$ detection limit in a four arcsecond diameter aperture of $K_s \sim 20$. More than 3,300 galaxies are identified in the K_s-band survey so far, of which $\gtrsim 550$ have $R-K_s \gtrsim 5$.

3 Photometric Redshift Analysis and Optical and Near-infrared Colors

Over the past several years, it has been demonstrated that distant galaxies may be accurately and reliably identified using photometric redshift techniques that incorporate optical and near-infrared broad-band photometry ([3, 16, 5]). For galaxies lacking strong emission or absorption features, we are still able to estimate redshifts based on the presence/absence of spectral discontinuities in broad-band optical and near-infrared colors. To identify distant red galaxies, we have adopted the photometric redshift technique developed originally by Lanzetta and collaborators ([9, 5]), and modified the program to account for the large number of stars that appear in wide-field surveys by including a suite of stellar templates—from early-type OB stars to late-type L and T dwarfs.

Comparison of photometric redshifts $z_{\rm phot}$ and spectroscopic redshifts $z_{\rm spec}$ at redshifts $0 \le z < 2.5$ for 67 objects with spectroscopic redshifts in the Hubble Deep Field South (HDFS) shows that the photometric redshifts are both accurate and reliable, with an RMS dispersion between the photometric and spectroscopic redshifts of $\Delta z/(1+z) \approx 0.1$ (Figure 1a). The accuracy and reliability of photometric redshift measurements allow us to study the galaxy two-point correlation function and the galaxy luminosity function as a function of redshift at $z \lesssim 2.5$ using the wide-field survey data. The lower precision of photometric redshift measurements may be compensated by the large sample size. We show in Figure 1b the redshift histogram of the H-band detected galaxies and of those with $I-H \gtrsim 3$ identified in the HDFS region. The curves indicate the predicted redshift distribution of the total and red populations based on the model that best fits the differential surface density measurements as

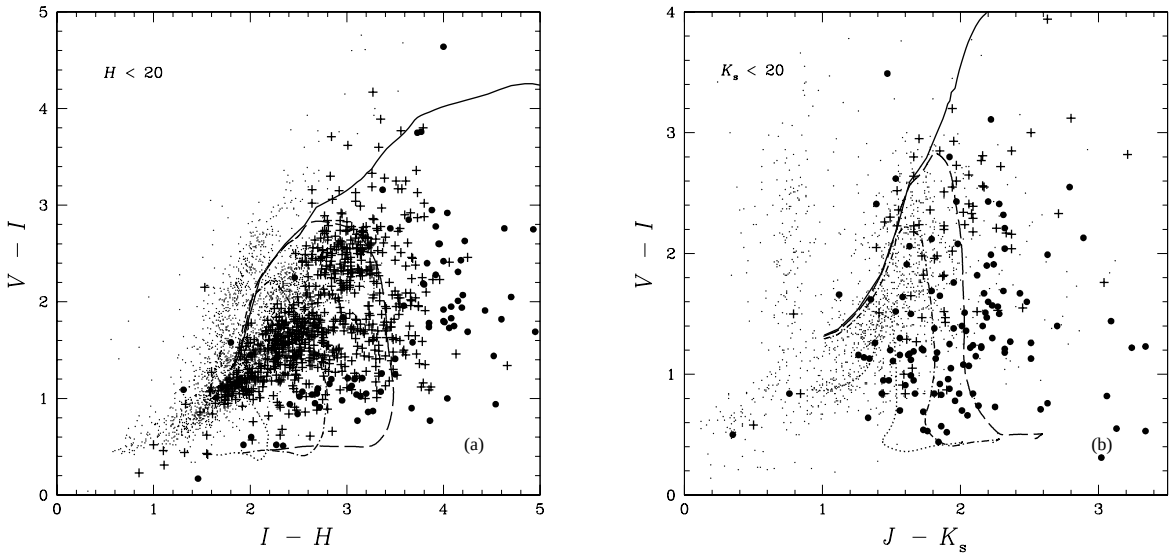

Figure 2: The $V-I$ vs. $I-H$ colors (a) and $V-I$ vs. $J-K_s$ (b) colors for objects identified in one of the survey fields. Different symbols represent objects at different redshifts according to the results of our photometric redshift analysis: $z \lesssim 0.75$ (dots), $0.75 \lesssim z \lesssim 1.0$ (circles), $1.0 \lesssim z \lesssim 1.5$ (crosses). The model curves show the loci of evolving population models with various star formation laws: a single burst with $z_f = 30$ (solid curve), exponentially declining with $\tau = 1\&2$ Gyr (dashed and dash-dotted curves), and continuous (dotted curve).

described below in § 4.1. The $I-H \gtrsim 3$ color criterion is determined based on predictions of various evolution scenarios to select evolved galaxies at $z \gtrsim 1$. It is analogous to a color selection of $R-K_s \gtrsim 5$ ([2]). Figure 1b shows that more than 6% of the H-band detected galaxies have $I-H \gtrsim 3$ and $z \gtrsim 1$.

We present the $V-I$ vs. $I-H$ color–color distribution of the H-band detected objects in Figure 2a and the $V-I$ vs. $J-K_s$ color–color distribution of the K_s-band detected objects in Figure 2b, along with predictions based on different star formation histories. Different symbols represent objects at different redshifts according to the results of our photometric redshift analysis. The general agreement between distributions of various model predictions and measurements of galaxies in our catalog, and the clear separation of the stellar sequence (which is most obvious in the $V-I$ vs. $J-K_s$ plot) suggest that most stars have been accurately identified in our survey fields. The large scatter in the $V-I$ colors (corresponding to the rest-frame UV colors at $z \gtrsim 1$) spanned by the galaxies of red $I-H$ or $J-K_s$ colors reveals a wide range of star formation histories for which our simple models provide only an idealized description. In particular, the large scatter in the $V-I$ colors for galaxies of $I-H \gtrsim 3$ or $J-K_s \gtrsim 1.9$ (indicative of redshifts $z \gtrsim 1$) suggest a significant amount of ongoing star formation in these galaxies. In addition, the small fraction of galaxies with $I-H \gtrsim 3$ and $V-I \gtrsim 3$ (or $J-K \gtrsim 2$ and $V-I \gtrsim 3$) suggests that there are few objects that may be adequately characterized as pure passively evolving systems formed at high redshifts.

4 Statistical Properties of Red Galaxies

4.1 Galaxy Number-Magnitude Relation

Figure 3a shows the number-magnitude relation of the H-band detected galaxies (open squares) and the H-band detected red galaxies (closed points) along with model predictions (curves) and previous measurements (open points). The number-magnitude relation of the H-band detected galaxies may be described using a local K-band luminosity function ([7]) with pure luminosity evolution expected from a 1 Gyr exponentially declining star formation rate model. To model the number-magnitude relation of the red population, we scale the luminosity function according to the population ratio of elliptical galaxies observed in the local universe and identify red galaxies as those brighter than $M_* - 1$ with a faint-end slope $\alpha = 1$, $M_*(\mathrm{red}) = M_* - 0.2$, and a space density $\phi_*(\mathrm{red}) = 0.15\phi_*$. We also

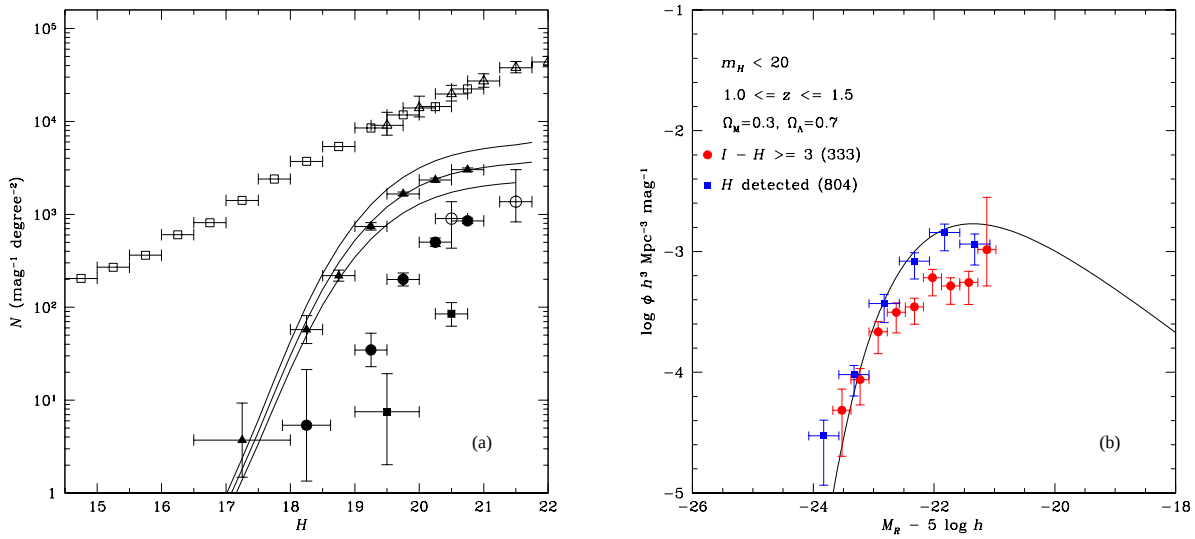

Figure 3: (a) The total (open squares) and red (closed points) galaxy differential surface density as a function of H-band magnitude in four of the survey fields. The open triangles are NICMOS measurements presented in [18]. The closed triangles, circles, and squares are the surface density measurements for $I - H \gtrsim 3$, 4 and 5, respectively. The error bars show the 95% confidence interval assuming Poisson statistics. The open circles at $H = 20.5$ and 21.5 are from the $R - H \gtrsim 5$ NICMOS sample in [19]. The curves show model predictions derived from a simple evolving population model as described in the text. (b) Rest-frame R-band luminosity function measurements of the H-band selected galaxies identified in two of the survey fields at redshifts between $z = 1$ and 1.5. The solid curve is a scaled CNOC2 luminosity function of color selected early-type galaxies at $z \sim 0.3$. There are 804 H-band detected galaxies with $m_H \lesssim 20$ and at $1.0 \lesssim z \lesssim 1.5$, 333 of which have $I - H \gtrsim 3$.

consider a number density evolution characterized by $(1 + z)^{-p}$ with $p = 0$, 0.5, and 1.0 (solid curves from top to bottom). Our measurements are consistent with previous surface density measurements both for the total and the red populations. Figure 3a shows that a luminosity evolution model with a mild space density evolution may explain the faint number counts.

The much steeper bright-end slope of the number-magnitude relation of the red galaxies indicates that most of the foreground ($z \lesssim 1$) galaxies have been effectively excluded from the red population and that the slope reflects the shape of the bright-end luminosity function of the red population. In addition, we find that red galaxies with $I - H \gtrsim 3$ constitute $\approx 20\%$ of the H-band detected galaxies at $H \lesssim 21$, but only $\approx 2\%$ at $H \lesssim 19$. A strong field-to-field variation in the surface density of the red population is directly observed in our survey, which is expected according to the results of angular clustering analysis of these red galaxies ([4, 14, 6]). We estimate a mean surface density of ≈ 1 arcmin^{-2} with an rms dispersion of ≈ 0.4 arcmin^{-2} for red galaxies brighter than $H = 20.5$. Finally, the consistent slopes between the red subsamples suggest similar underlying luminosity functions.

4.2 Galaxy Luminosity Function

Various deep redshift surveys have yielded consistent measurements of the luminosity function for galaxies at $z \lesssim 0.75$ (see e.g. [11, 10]), but it becomes exceedingly difficult beyond this redshift range both because galaxies become even fainter and because bright sky lines make accurate spectroscopic redshift identifications challenging. Despite a lower precision, the large number of distant galaxies expected from a wide-field multi-color survey allow us to obtain statistically significant estimates of various galaxy properties using photometric redshift measurements. Here we present the first measurements of the galaxy luminosity function at $1.0 \lesssim z \lesssim 1.5$ based on photometric redshifts.

Figure 3b shows the rest-frame R-band luminosity functions of the total H-band selected sample and galaxies with $I - H \gtrsim 3$ in two of our survey fields. At $z \sim 1.2$, the observed-frame H-band roughly corresponds to the rest-frame R-band, therefore the calculation does not rely heavily on the adopted templates to determine the k-correction. We calculate the luminosity function in each magnitude bin

using the $1/V_{\rm max}$ method, where $V_{\rm max}$ is estimated as the comoving volume accessible by a galaxy in the sample based on its absolute magnitude. Errors are calculated using a bootstrap method, including sampling errors and measurement uncertainties in photometric redshift, galaxy photometry, and colors. Comparison of the luminosity functions of the total and red populations shows that red galaxies dominate the bright galaxy population at $z \gtrsim 1$. Specifically, the space densities of the two populations are statistically identical at the bright end. The space densities of red galaxy and galaxies with bluer $I-H$ colors become comparable at around M_*. Finally, our H-band survey is insensitive to sub-$L*$ galaxies, and so we cannot constrain the faint-end slope of the luminosity function.

To assess luminosity function evolution, we compare our measurements with those presented in [10]. The solid curve in Figure 3b shows a scaled CNOC2 luminosity function of color selected early-type galaxies at $z \sim 0.3$. First, we estimate a luminosity evolution using the same 1-Gyr exponentially declining star formation model and find that $M_{R_*}(z \sim 1.2) = M_{R_*}(z \sim 0.3) - 0.8$. Next, we find that a scaling factor in the space density $\phi_*(z = 1.2) = 0.55\,\phi_*(z = 0.3)$ is necessary to match the curve with our measurements, consistent with the results of the number-magnitude analysis. However, the degree to which the CNOC2 and LCIRs samples probe the same galaxy population remains uncertain. In summary, the results of number count studies and luminosity function measurements indicate that most early-type galaxies were already in place by $z \sim 1.2$ with a modest space density evolution and a mild luminosity evolution over that expected from passive evolution.

Acknowledgements. This research was supported by the National Science Foundation under grant AST-9900806. H.-W. Chen acknowledges partial support from an International Travel Grant provided by the American Astronomy Society. The CIRSI camera was made possible by the generous support of the Raymond and Beverly Sackler Foundation.

References

[1] Beckett et al. 1998, in Infrared Astronomical Instrumentation, ed. Fowler, A.M., SPIE, 3354, p14

[2] Chen, H.-W., McCarthy, P. J., & Marzke, R. O. et al. 2001, ApJ submitted (astro-ph/0108171)

[3] Connolly, A. J., Szalay, A. S. et al. 1997, ApJ, 486, L11

[4] Daddi, E., Cimmatti, A., Pozzetti, L., & Hoekstra, H. et al. 2000, A&A, 361, 535

[5] Fernández-Soto, A., Lanzetta, K. M., & Yahil, A. 1999, ApJ, 513, 34

[6] Firth, A. E., Somerville, R., McMahon, R. G. et al., 2001, MNRAS submitted (astro-ph/0108182)

[7] Gardner, J. P., Sharples, R. M., Frenk, C. S., & Carrasco, B. E. 1997, ApJ, 480, L99

[8] Kauffmann, G. & Charlot, S. 1998, MNRAS, 297, L23

[9] Lanzetta, K. M., Yahil, A., & Fernández-Soto, A. 1996, Nature, 381, 759

[10] Lin, H., Yee, H. K. C., Carlberg, R. G. et al. 1999, ApJ, 518, 533

[11] Marzke, R. O., da Costa, L. N. et al. 1998, ApJ, 503, 617

[12] Marzke, R. O. et al. 1999, in A.S.P. Conf. Series vol. 191, p. 148

[13] McCarthy, P. J. et al. 2001a, in the Proceedings of "Deep Fields" (astro-ph/0011499)

[14] McCarthy, P. J., Carlberg, R. G., Chen, H.-W., & Marzke, R. O. et al. 2001b, ApJL, 560, 131

[15] Persson, S. E., Murphy, C. D., Gunnels, S., Birk, C. et al. 2001, AJ submitted

[16] Sawicki, M. J., Lin, H., & Yee, H. K. C. 1997, AJ, 113, 1

[17] Totani, T. & Yoshii, J. 1997, ApJ, 501, L177

[18] Yan, L., McCarthy, P., Storrie-Lombardi, L., Weymann, R. J. 1998, ApJ, 503, 19

[19] Yan, L., McCarthy, P., Weymann, R., Malkan, M. et al. 2000, AJ, 120, 575